THE JOURNAL OF BIOLOGICAL CHEMISTRY VOL. 289, NO. 3, pp. 1852–1865, January 17, 2014
Published in the U.S.A.

Growth Arrest by the Antitumor Steroidal Lactone Withaferin A in Human Breast Cancer Cells Is Associated with Down-regulation and Covalent Binding at Cysteine 303 of β-Tubulin*

Received for publication, June 25, 2013, and in revised form, December 2, 2013 Published, JBC Papers in Press, December 2, 2013, DOI 10.1074/jbc.M113.496844

Marie L. Antony[‡], Joomin Lee[‡], Eun-Ryeong Hahm[‡], Su-Hyeong Kim[‡], Adam I. Marcus[§], Vandana Kumari[¶], Xinhua Ji[¶], Zhen Yang[§], Courtney L. Vowell[‖], Peter Wipf[‖], Guy T. Uechi[‡‡], Nathan A. Yates[**‡‡], Guillermo Romero[‡], Saumendra N. Sarkar[‡‡§§], and Shivendra V. Singh[‡ ‡‡1]**

*From the Departments of [‡]Pharmacology and Chemical Biology and [§§]Microbiology and Molecular Genetics, University of Pittsburgh School of Medicine, and the [‖]Department of Chemistry, University of Pittsburgh, Pittsburgh, Pennsylvania 15260, the [§]Department of Hematology and Medical Oncology, Emory University, Atlanta, Georgia 30322, the [¶]Biomolecular Structure Section, Center for Cancer Research, NCI, Frederick, Maryland 21702, and the **Biomedical Mass Spectrometry Center, University of Pittsburgh School of Medicine, and the [‡‡]University of Pittsburgh Cancer Institute, Pittsburgh, Pennsylvania 15213*

Background: The tubulin microtubule network remains an attractive anticancer target.
Results: The antitumor steroidal lactone withaferin A (WA) down-regulates tubulin and binds to Cys^{303} of β-tubulin.
Conclusion: Tubulin is a novel target of WA-mediated growth arrest in human breast cancer cells.
Significance: Favorable safety and pharmacokinetic profiles merit clinical investigation of WA for prevention and/or treatment of breast cancer.

Withaferin A (WA), a C_5,C_6-epoxy steroidal lactone derived from a medicinal plant (*Withania somnifera*), inhibits growth of human breast cancer cells *in vitro* and *in vivo* and prevents mammary cancer development in a transgenic mouse model. However, the mechanisms underlying the anticancer effect of WA are not fully understood. Herein, we report that tubulin is a novel target of WA-mediated growth arrest in human breast cancer cells. The G_2 and mitotic arrest resulting from WA exposure in MCF-7, SUM159, and SK-BR-3 cells was associated with a marked decrease in protein levels of β-tubulin. These effects were not observed with the naturally occurring C_6,C_7-epoxy analogs of WA (withanone and withanolide A). A non-tumorigenic normal mammary epithelial cell line (MCF-10A) was markedly more resistant to mitotic arrest by WA compared with breast cancer cells. Vehicle-treated control cells exhibited a normal bipolar spindle with chromosomes aligned along the metaphase plate. In contrast, WA treatment led to a severe disruption of normal spindle morphology. NMR analyses revealed that the A-ring enone in WA, but not in withanone or withanolide A, was highly reactive with cysteamine and rapidly succumbed to irreversible nucleophilic addition. Mass spectrometry demonstrated direct covalent binding of WA to Cys^{303} of β-tubulin in MCF-7 cells. Molecular docking indicated that the WA-binding pocket is located on the surface of β-tubulin and characterized by a hydrophobic floor, a hydrophobic wall, and a charge-balanced hydrophilic entrance. These results provide novel insights into the mechanism of growth arrest by WA in breast cancer cells.

Constituents of Ayurvedic medicine, which has been safely followed for thousands of years in India, continue to draw attention for identification of small molecules potentially useful for the treatment and prevention of chronic diseases (1). *Withania somnifera* (also known as Ashwagandha or Indian winter cherry) is one such medicinal plant, whose leaf and root are integral components of the Ayurvedic remedies used for the healing of different conditions, including inflammation, arthritis, asthma, and hypertension (2). Preclinical experimental evidence exists indicating that *W. somnifera* leaf and root extracts are inhibitory to cancer (3, 4). For example, chemically induced forestomach and skin tumorigenesis in mice was inhibited significantly following administration of *W. somnifera* root (4).

The anticancer effect of *W. somnifera* is ascribed to steroidal lactones collectively known as withanolides (5, 6). Even though multiple withanolides with side chain alterations have been isolated from *W. somnifera*, withaferin A (WA),[2] a C_5,C_6-epoxy steroidal lactone, is one of the best characterized and the most active compound, exerting anti-inflammatory, antiproliferative, pro-apoptotic, anti-invasive, and anti-angiogenic effects (7). The *in vivo* anticancer effect of WA was initially shown against Ehrlich ascites cells in the early 1970s (8). This compound was later shown to be a potent *in vivo* radiosensitizer (9).

* This work was supported, in whole or in part, by National Institutes of Health Grants R01 CA142604-04 and R01 CA129347-07 from NCI (to S. V. S.) and by the Intramural Research Program of the Center for Cancer Research, NCI, National Institutes of Health (to X. J.). The work performed in the University of Pittsburgh Cancer Institute Flow Cytometry Facility and Cancer Biomarkers Facility was supported in part by National Institutes of Health Cancer Center Support Grant P30CA047904 from NCI.

[1] To whom correspondence should be addressed: University of Pittsburgh Cancer Institute, 2.32A Hillman Cancer Center, 5117 Centre Ave., Pittsburgh, PA 15213. Tel.: 412-623-3263; E-mail: singhs@upmc.edu.

[2] The abbreviations used are: WA, withaferin A; ER, estrogen receptor; ROS, reactive oxygen species; WE, withanone; WLA, withanolide A; DMSO, dimethyl sulfoxide.

Subsequent work from different laboratories, including our own, has established that WA treatment not only retards the growth of different types of human tumor cells *in vitro* and *in vivo* but also prevents chemically induced as well as spontaneous cancer development in experimental rodents (10–15). For example, chemically induced oral carcinogenesis in hamsters was inhibited significantly by WA administration (13). Recent studies from our own laboratory have revealed that WA administration significantly inhibits burden (affected area) of ductal carcinoma *in situ* as well as invasive mammary cancer in mouse mammary tumor virus-*neu* transgenic mice in association with inhibition of glycolysis (14).

The mechanism by which WA inhibits the growth of tumor cells is not fully understood, but known molecular effects potentially contributing to its anticancer activity include (*a*) G_2-M phase cell cycle arrest (16); (*b*) apoptosis induction (10, 12, 17); (*c*) inhibition of proteasomes (11); (*d*) suppression of NF-κB, STAT3, and estrogen receptor (ER)-α (5, 18–20); and (*e*) inhibition of processes relevant to metastatic spread of tumors, including neo-angiogenesis and cell migration (21, 22). Considerable progress has been made toward our understanding of the mechanism by which WA induces apoptotic cell death in cancer cells (10, 12, 17). Molecular events associated with WA-induced apoptosis in human breast cancer cells include inhibition of complex III of mitochondrial respiration, leading to suppression of oxidative phosphorylation and production of reactive oxygen species (ROS), activation of multidomain pro-apoptotic proteins Bax and Bak, and ensuing cell death (17). In contrast, the molecular basis for the cell cycle arrest resulting from WA exposure is poorly defined. In this study, we demonstrate, for the first time, that β-tubulin is a novel target of WA-mediated growth arrest in breast cancer cells.

EXPERIMENTAL PROCEDURES

Reagents—Purified tubulin from MCF-7 cells was purchased from Cytoskeleton (Denver, CO). WA (purity of 99%) was purchased from Enzo Life Sciences (Farmingdale, NY), whereas its analogs withanone (WE; purity of 95.6%) and withanolide A (WLA; purity of 96.7%) were purchased from ChromaDex (Irvine, CA). Stock solutions of the withanolides were prepared in dimethyl sulfoxide (DMSO), and an equal volume of DMSO was added to the controls. The final concentration of DMSO did not exceed 0.1%. Reagents for cell culture and Alexa Fluor 488- and Alex Fluor 568-conjugated goat anti-mouse antibodies were purchased from Invitrogen. McCoy's 5A medium was from Mediatech (Manassas, VA). Mouse monoclonal antibodies against α- and β-tubulin, anti-actin antibody, and DAPI were purchased from Sigma-Aldrich. The rabbit polyclonal antibody against β-tubulin was purchased from Abcam (Cambridge, MA). Anti-securin antibody was purchased from MBL International (Woburn, MA), whereas an antibody specific for detection of Ser^{10}-phosphorylated histone H3 was from Cell Signaling Technology (Danvers, MA). Proteasomal inhibitor MG132 was purchased from EMD Millipore (Billerica, MA). Protein A/G PLUS-agarose beads were purchased from Santa Cruz Biotechnology (Santa Cruz, CA).

Cell Lines and Cell Viability Assays—MCF-7, SK-BR-3, and MCF-10A cells were obtained from American Type Culture Collection (Manassas, VA) and maintained as suggested by the supplier or as described previously (23). The SUM159 cell line was purchased from Asterand (Detroit, MI) and cultured in Ham's F-12 medium supplemented with 5% fetal bovine serum, 1 μg/ml hydrocortisone, 5 μg/ml insulin, and 10 mM HEPES. MCF-7 cells stably transfected with the pcDNA3.1 empty vector or the same vector encoding copper/zinc superoxide dismutase have been described by us previously (17). The effect of the withanolides on the viability of MCF-7 and SUM159 cells was determined by trypan blue dye exclusion assay as described by us previously (24). The effect of the withanolides on cell proliferation was determined using the CellTiter 96® AQ_{ueous} non-radioactive cell proliferation assay kit from Promega. Briefly, the cells ($0.7\sim1 \times 10^3$ cells/well) were seeded in 96-well plates in triplicate or quadruplicate, incubated overnight, and treated with DMSO (control) or withanolides (1, 2, or 4 μM) for 24, 48, and 72 h. After treatment, the absorbance of the resultant formazan product was measured at 492 nm using a microplate reader.

Flow Cytometric Analysis of Cell Cycle Distribution—SUM159 cells (1×10^5 cells/well in 6-well plates) and MCF-7 cells (5×10^5 cells/dish in 6-cm culture dishes) were plated in triplicate. After overnight incubation, the cells were treated with DMSO (control) or 2 μM WA, WE, or WLA for 8 or 24 h, followed by fixation in 70% ethanol overnight at 4 °C. Fixed cells were washed with PBS, stained with propidium iodide, and analyzed using a BD Accuri™ C6 flow cytometer (BD Biosciences) or a CyAn™ ADP analyzer (Beckman Coulter, Brea, CA). In some cell cycle distribution studies, the DMSO-treated control and WA-treated MCF-7 cells (5×10^5 cells/dish in 6-cm culture dishes) were also immunostained for α- and β-tubulin proteins to quantify their cell cycle phase-specific levels.

Western Blotting—Details of Western blotting have been described elsewhere (25). Immunoreactive bands were detected by the enhanced chemiluminescence method. Densitometric quantification was done using UN-SCAN-IT version 5.1 (Silk Scientific Inc., Orem, UT).

Flow Cytometric Quantitation of Mitotic Fraction—Quantitation of the mitotic fraction in control and WA-treated cells was achieved by flow cytometry after staining the cells with propidium iodide and anti-phospho-Ser^{10} histone H3 antibody. The cells (2.5×10^3 cells/well) were seeded in 6-well plates, incubated overnight, and exposed to DMSO or 2 μM WA for 8 or 24 h. The cells were collected by trypsinization and fixed in 70% ethanol at 4 °C by overnight incubation. Subsequently, the cells were permeabilized with 0.25% Triton X-100 for 15 min at room temperature, incubated with Alexa Fluor 488-conjugated phospho-Ser^{10} histone H3 antibody for 1 h, stained with propidium iodide for 30 min at room temperature, and analyzed using the BD Accuri C6 flow cytometer.

Real-time Quantitative RT-PCR—Total RNA was isolated using the RNeasy kit (Qiagen), and cDNA was synthesized and reverse-transcribed using an oligo$(dT)_{20}$ primer and SuperScript III reverse transcriptase (Invitrogen). PCR was performed using SYBR Green Master Mix in an ABI StepOnePlus real-time PCR system (Applied Biosystems). The primers used

were: as follows: α-tubulin, 5′-CTCCAGGGCTTCTTGGTTTTCC-3′ (forward) and 5′-TTTCACCATCTGGTTGGCTGGC-3′ (reverse); β_1-tubulin, 5′-CTCCAGCCTCTGGGGCGC-3′ (forward) and 5′-ATTTGCCACCTGTGGCTTCA-3′ (reverse); and glyceraldehyde-3-phosphate dehydrogenase, 5′-TGATGACATCAAGAAGGTGGTGAAG-3′ (forward) and 5′-TCCTTGGAGGCCATGTGGGCCAT-3 (reverse). The cycling conditions for α- and β_1-tubulin were as follows: 95 °C for 10 min, followed by 35 cycles at 95 °C for 30 s, 62 °C for 30 s, and 72 °C for 30 s. Relative gene expression was calculated using the method described by Livak and Schmittgen (26).

Immunofluorescence Microscopy for α- and β-Tubulin—MCF-7, SUM159, SK-BR-3, and MCF-10A cells ($7\sim9 \times 10^4$ cells/well) were plated on glass coverslips in 12-well plates and allowed to attach overnight. After a 24-h treatment with DMSO (control) or 2 μM WA, the cells were fixed in 3% paraformaldehyde, followed by permeabilization with Triton X-100. Cells were incubated with blocking buffer containing bovine serum albumin in PBS for 30 min at room temperature, followed by incubation with anti-α- or anti-β-tubulin antibody overnight at 4 °C. The cells were then incubated with Alexa Fluor 488- or Alexa Fluor 568-conjugated secondary antibody. DAPI was used to stain nuclear DNA. Coverslips were mounted using Antifade Fluoromount, and the images were captured using an Olympus FluoView 1000 confocal microscope with 63 × 1.45 numerical aperture objective magnification and 565- and 488-nm laser wavelengths.

Kinetic Analysis of the Thiol Reactivity of Withanolides by NMR—Each reaction was performed under an atmosphere of dry N_2 or argon. ^{1}H NMR spectra were recorded on a Bruker AVANCE III 500-MHz instrument. Samples were auto-tuned and matched (atma), auto-shimmed (topshim), and calibrated to the residual solvent peak. $CDCl_3$ and CD_2Cl_2 were filtered through basic Al_2O_3 immediately prior to sample preparation. DMSO-d_6 was deoxygenated before use. Chemical shifts (δ) are reported in parts/million with the residual solvent peak used as an internal standard: δ ^{1}H, 7.26 ($CDCl_3$), 5.32 (CD_2Cl_2), and 2.50 (DMSO-d_6).

WE (0.0092 g, 0.020 mmol) was dissolved in DMSO-d_6 (300 μl) in a J Young NMR tube, and the ^{1}H NMR spectrum was recorded as a standard. Cysteamine (2-aminoethanethiol; 0.0042 g, 0.053 mmol) was added, and the mixture was reanalyzed by ^{1}H NMR at 5-min and 5-h time points. An aliquot (15 μl) of the solution was then transferred into a second NMR tube containing $CDCl_3$ (300 μl), and a new spectrum was recorded. No difference was observed at the enone peaks at 6.58 and 5.64 ppm.

Cysteamine (0.0034 g, 0.042 mmol) was dissolved in DMSO-d_6 (300 μl) in a J Young NMR tube, and WLA (0.0085 g, 0.018 mmol) was added. Independently, a spectrum of WLA was recorded as a standard. The mixture of WLA and cysteamine was analyzed by ^{1}H NMR at 5 min and 5 h. An aliquot (20 μl) of the solution was then transferred into a second NMR tube containing $CDCl_3$ (400 μl), and a new spectrum was recorded. The enone peaks at 6.58 and 5.64 ppm decreased by 25% after 5 min of incubation, but these peaks were present in full intensity after 5 h.

WA (0.010 g, 0.021 mmol) was dissolved in DMSO-d_6 (300 μl) in a J Young NMR tube, and the spectrum was recorded as a standard. Cysteamine (0.0038 g, 0.049 mmol) was added, and the mixture was analyzed by ^{1}H NMR at 5-min and 5-h time points. A complete disappearance of the enone olefin peaks was observed. An aliquot (20 μl) of the solution was then transferred into a second NMR tube containing $CDCl_3$ (400 μl), and a new spectrum was recorded, but no reversal in the enone addition reaction was observed. The enone peaks at 7.08 and 6.12 ppm disappeared 5 min after thiol addition and did not reappear.

Mass Spectrometric Detection of Covalent Binding of WA to β-Tubulin—First, an *in vitro* experiment was performed by incubating 2 μg of purified human tubulin (Cytoskeleton) for 1–2 h at 37 °C with either DMSO (control) or 8 μM WA. In the second experiment, 10^6 MCF-7 cells were plated in a 10-cm culture dish and allowed to attach. The cells were then treated with DMSO or 2 μM WA for 24 h at 37 °C and lysed. An aliquot containing 500 μg of lysate protein was precleared with 100 μl of protein A/G PLUS-agarose beads and then incubated with 10 μg of agarose-conjugated anti-β-tubulin antibody at 4 °C. Samples from both experiments (*in vitro* incubation and MCF-7 cells) were denatured and subjected to SDS-PAGE. The Coomassie Blue-stained gel bands were excised, destained, and digested with trypsin as described by Shevchenko *et al.* (27).

The *in vitro* incubated samples were analyzed by MALDI-TOF with full-scan mass spectra with a mass range of *m/z* 800–4000 in reflectron mode (AB Sciex Model 4800) at a resolution of 18,000 at *m/z* 2465. The mass accuracy was maintained below 20 ppm, and spectra from 400 individual laser shots were averaged. The same *in vitro* incubated samples were also analyzed by LC-MS/MS. The peptides were sequenced using a Waters nanoACQUITY UPLC system (Models 186016006 and 186016002) coupled to an Orbitrap Velos Pro hybrid linear quadrupole ion trap and orbitrap mass spectrometer (Thermo Fisher). Full-scan mass spectra with a mass range of *m/z* 300–2000 were acquired in profile mode in the orbitrap at a resolution of 60,000. Chromatographic separation was performed at a constant flow rate of 0.3 μl/min using a binary solvent system (solvent A, 0.1% formic acid; solvent B, acetonitrile and 0.1% formic acid) and a linear gradient program (0–3 min, 5% solvent B; 3–60 min, 5–55% solvent B; 60–61 min, 55–95% solvent B; 61–66 min, 95% solvent B; 66–67 min, 95–5% solvent B; and 67–87 min, 5% solvent B). The data-dependent acquisition mode was used to collect MS/MS spectra for the most intense ions (up to nine) from the preceding high-resolution full-scan orbitrap mass spectrum.

Immunoprecipitated β-tubulin from WA-treated and control (DMSO-treated) MCF-7 cells was analyzed by LC-MS/MS to determine the relative abundance of the modified and unmodified forms of Cys^{303}. Briefly, a linear ion trap mass spectrometer was used to record tandem mass spectra for specific peptide ions corresponding to the *m/z* of modified and unmodified tryptic peptides of β-tubulin. The identity of each β-tubulin peptide was confirmed by manual inspection of the product ion spectra that were identified by a SEQUEST database search (Thermo Fisher Proteome Discoverer 1.3.0.339) that considered methionine oxidation and the addition of 470.6 Da to cys-

teine as variable modifications. The relative abundance of the modified and unmodified Cys^{303} peptides (NMM#AAC*DPR) was computed by integrating the selected ion chromatograms for b_7^+ product ion at *m/z* 1223.6 and *m/z* 753.2, respectively.

Molecular Docking—Human β-tubulin shares ~95% sequence identity with bovine β-tubulin. The bovine β-tubulin structure (Protein Data Bank ID 4IHJ) (28) was used as a template to model human β-tubulin using the Phyre2 server (29). The coordinates of WA, WE, and WLA were obtained from the PubChem Database (SID 11034, 103600366, and 103600367, respectively). WA, WE, or WLA was docked as the ligand of the human β-tubulin model using AutoDock 4.2 (30). During docking simulations, the ligand was kept fully flexible (rotation about the single bonds), and Gasteiger charges were applied. A grid map of 60 × 60 × 60 points with a spacing of 0.375 Å around Cys^{303} of β-tubulin was used, and grid potential maps were calculated using AutoGrid v4.2, one of the utility programs of AutoDock. The Lamarckian genetic algorithm, which uses a combination of a genetic algorithm and a local search, was used as the conformational search method for the docking simulation. The generated conformations were clustered with a tolerance of a 1.5-Å root mean square deviation, and the cluster with the highest number of conformations was selected for each of the human β-tubulin·WA, β-tubulin·WE, and β-tubulin·WLA complexes. Among the three complexes, only human β-tubulin·WA was compatible with the formation of a Cys^{303}-WA adduct. Therefore, a dihydro-WA model was created to mimic the Cys^{303}-WA adduct conformation. Dihydro-WA was docked as the ligand of the human β-tubulin model following the same protocol described above. The generated conformations were clustered also with a tolerance of 1.5-Å root mean square deviation, and the cluster with highest number of conformations was selected for the human β-tubulin·dihydro-WA complex.

Modeling of the Cys^{303}-WA Adduct of Human β-Tubulin—Protein-bound WA and dihydro-WA exhibit virtually the same binding mode for the protein, compatible with the covalent conjugate addition of the Cys^{303} thiol to the enone of WA. To mimic the Cys^{303}-WA adduct of human β-tubulin, the docked conformation of dihydro-WA was used. The Cys^{303} thiol of human β-tubulin was attached covalently at the β-carbon of dihydro-WA, and the structure was optimized using the MacroModel module (version 9.6, Schrödinger, LLC). The OPLS_2005 force field with efficient continuum solvation models was used during energy minimization. The illustration was prepared with PyMOL (Delano Scientific, LLC).

RESULTS

Effect of Withanolides on Cell Viability—We have shown previously that the viability of the MCF-7 cell line, which is a well characterized cellular model for ER-α-positive breast cancers, is decreased significantly after 24 h of exposure to WA, with an IC_{50} of ~2 μM (12). Notably, pharmacokinetic studies in BALB/c mice have revealed that the peak plasma concentration of WA is ~1.8 μM after a single intraperitoneal injection of 4 mg of WA/kg of body weight (15). In this study, we determined the effects of WA and its naturally occurring C_6,C_7-epoxy analogs WE and WLA (Fig. 1*A*) on the viability of MCF-7 cells and a triple-negative human breast cancer cell line (SUM159). Triple-negative breast cancers are largely unresponsive to clinically available targeted therapies and have the worse prognosis among different subtypes of breast cancer (31). The viability of MCF-7 cells (data not shown) as well as SUM159 cells (Fig. 1*B*) was decreased in the presence of WA. Statistically significant inhibition of cell viability upon treatment with WA was evident as early as 8 h post-treatment in both cell lines. The C_6,C_7-epoxy analogs were either inactive or relatively less active compared with WA in trypan blue dye exclusion assay.

Effect of Withanolides on Breast Cancer Cell Proliferation—Next, we determined the effects of the withanolides on cell proliferation using MCF-7 cells (Fig. 1*C*), SUM159 cells (Fig. 1*C*), and the ER-negative cell line SK-BR-3 (data not shown). Similar to cell viability data, WA exhibited a maximum inhibitory effect on the proliferation of each cell line compared with WE or WLA (Fig. 1*C*). In addition, the SUM159 cell line was relatively more sensitive to cell proliferation inhibition by WA compared with MCF-7 or SK-BR-3 cells especially at the 24-h time point. Together, these studies indicated that (*a*) WA inhibited the viability and proliferation of ER-positive (MCF-7), ER-negative (SK-BR-3), and triple-negative (SUM159) breast cancer cells and that (*b*) the location of the epoxide functional group might be a key structural determinant of the growth inhibitory effect of withanolides on breast cancer cells.

Effect of Withanolides on Cell Cycle Distribution in Breast Cancer Cells—WA-mediated inhibition of cell proliferation was associated with G_2-M phase cell cycle arrest in MCF-7, SUM159, and SK-BR-3 cells (Fig. 2*A*). The G_2-M phase cell cycle arrest was not evident when the MCF-7 or SUM159 cells were exposed to WE (Fig. 2*B*) or WLA (data not shown). The effect of WE or WLA on cell cycle distribution was not determined in SK-BR-3 cells.

Because flow cytometric analysis of DNA content can not distinguish G_2 phase and mitotic cells, Western blotting was performed for securin and Ser^{10}-phosphorylated histone H3 to determine the effect on mitotic population. Ser^{10}-phosphorylated histone H3 is a sensitive marker for mitotic cells, whereas securin is a substrate for a multisubunit ubiquitin ligase complex (anaphase-promoting complex/cyclosome) essential for initiation of anaphase as well as mitotic exit (32, 33). Exposure of SUM159 cells to WA resulted in accumulation of securin protein and increased Ser^{10} phosphorylation of histone H3 (Fig. 2*C*). These results were consistent with our previous observations in MCF-7 cells exhibiting mitotic arrest after treatment with WA (16).

WA-mediated mitotic arrest was confirmed by flow cytometric quantitation of Ser^{10}-phosphorylated histone H3 (Fig. 2*D*). The mitotic fraction (identified by *arrows* in Fig. 2*D*) was increased significantly after a 8- or 24-h treatment of MCF-7 cells (Fig. 2*E*), SUM159 cells (Fig. 2*E*), and SK-BR-3 cells (data not shown) with 2 μM WA compared with vehicle-treated control cells. Collectively, these results indicated that breast cancer cells were arrested in G_2 as well as mitotic phases after treatment with WA.

Effect of Withanolides on Tubulin Protein Levels in Breast Cancer Cells—Because microtubules consisting of α- and β-tubulin heterodimers play an important role in mitosis (34), it was

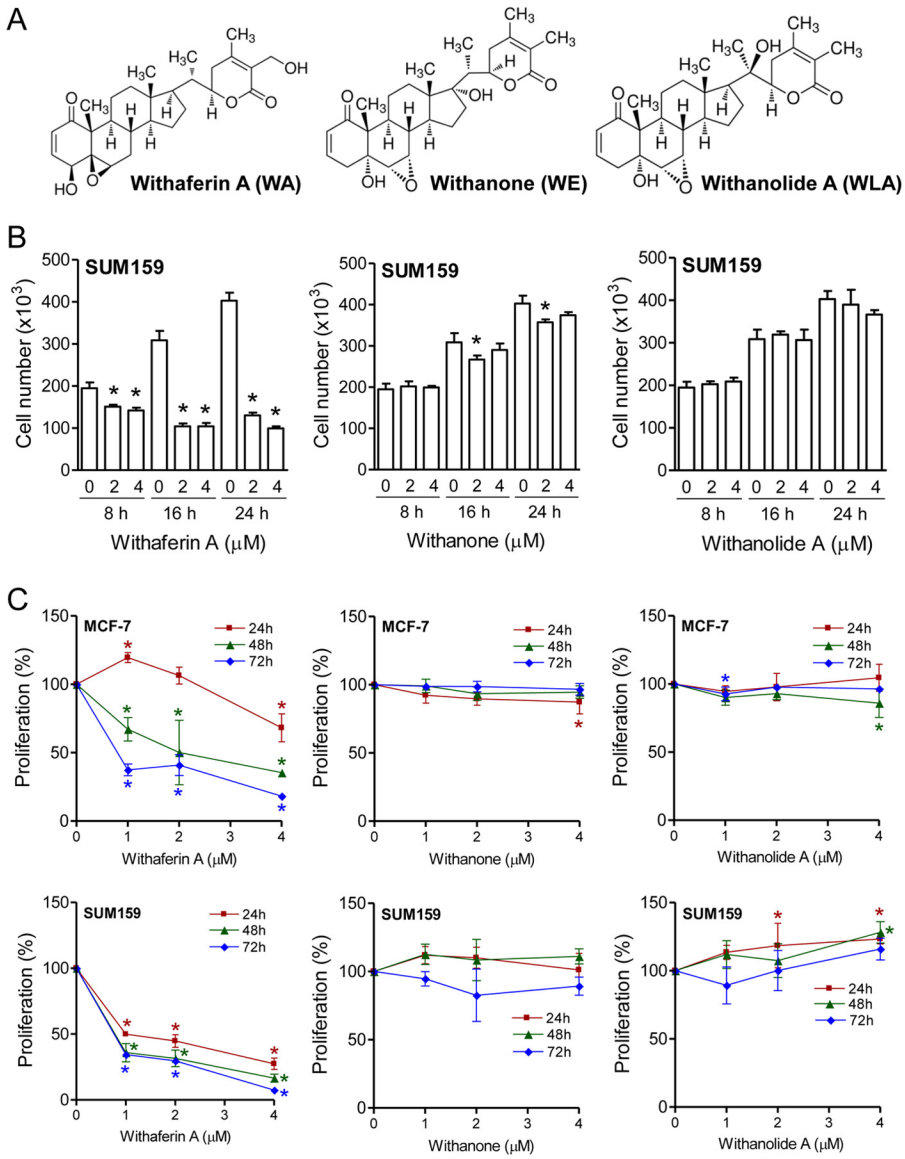

FIGURE 1. **WA is relatively more active than WE or WLA against human breast cancer cells.** *A*, chemical structures of WA, WE, and WLA. *B*, effect of withanolides (8-, 16-, or 24-h treatment) on the viability of SUM159 cells as determined by trypan blue dye exclusion assay. *C*, effect of withanolides (24-, 48-, or 72-h treatment) on proliferation of MCF-7 and SUM159 cells. Results shown are means ± S.D. ($n = 3–4$). *, significantly different ($p < 0.05$) compared with the corresponding control by one-way analysis of variance, followed by Dunnett's test. Experiments were repeated at least twice with similar results. Representative data from one such experiment are shown.

of interest to determine whether WA targets tubulin. Exposure of MCF-7, SUM159, and SK-BR-3 cells to WA resulted in a decrease in the protein levels of both α- and β-tubulin (Fig. 3*A*). However, the effect of WA was relatively more pronounced on the β-tubulin protein than on the α-isoform in each cell line (Fig. 3*B*). WE or WLA treatment did not have an appreciable effect on the protein level of either α-tubulin (data not shown) or β-tubulin (Fig. 3, *C* and *D*).

The WA-mediated decrease in α-tubulin (Fig. 4, *A* and *B*) and β-tubulin (Fig. 4, *C* and *D*) proteins was confirmed by flow cytometry using MCF-7 cells. Cell cycle phase-specific analysis of α-tubulin revealed suppression of its level only in the G_0-G_1 phase cells (Fig. 4*B*). In contrast, the level of β-tubulin was decreased in all phases of the cell cycle, although the difference from the control did not reach statistical significance in the G_2-M phase cells (Fig. 4*D*).

Next, we designed experiments to elucidate the mechanism underlying the decline in tubulin protein levels in WA-treated cells. Expression of α- and β_1-tubulin mRNAs was significantly and dose-dependently decreased after a 24-h treatment of MCF-7 and SUM159 cells with WA (Fig. 4*E*). Moreover, the decrease in the protein levels of α- and β-tubulin resulting from WA exposure (24-h treatment) was partially reversible in the presence of proteasomal inhibitor MG132 (Fig. 4*F*). These results indicated the involvement of both transcriptional repression and proteasomal degradation in WA-mediated suppression of α-and β-tubulin proteins.

WA Treatment Disrupts the Microtubule Network in Breast Cancer Cells—The microtubule network is critical for cell cycle progression during mitosis and for cell signaling during interphase (34); therefore, we determined the effect of WA treatment on microtubules by confocal microscopy after immuno-

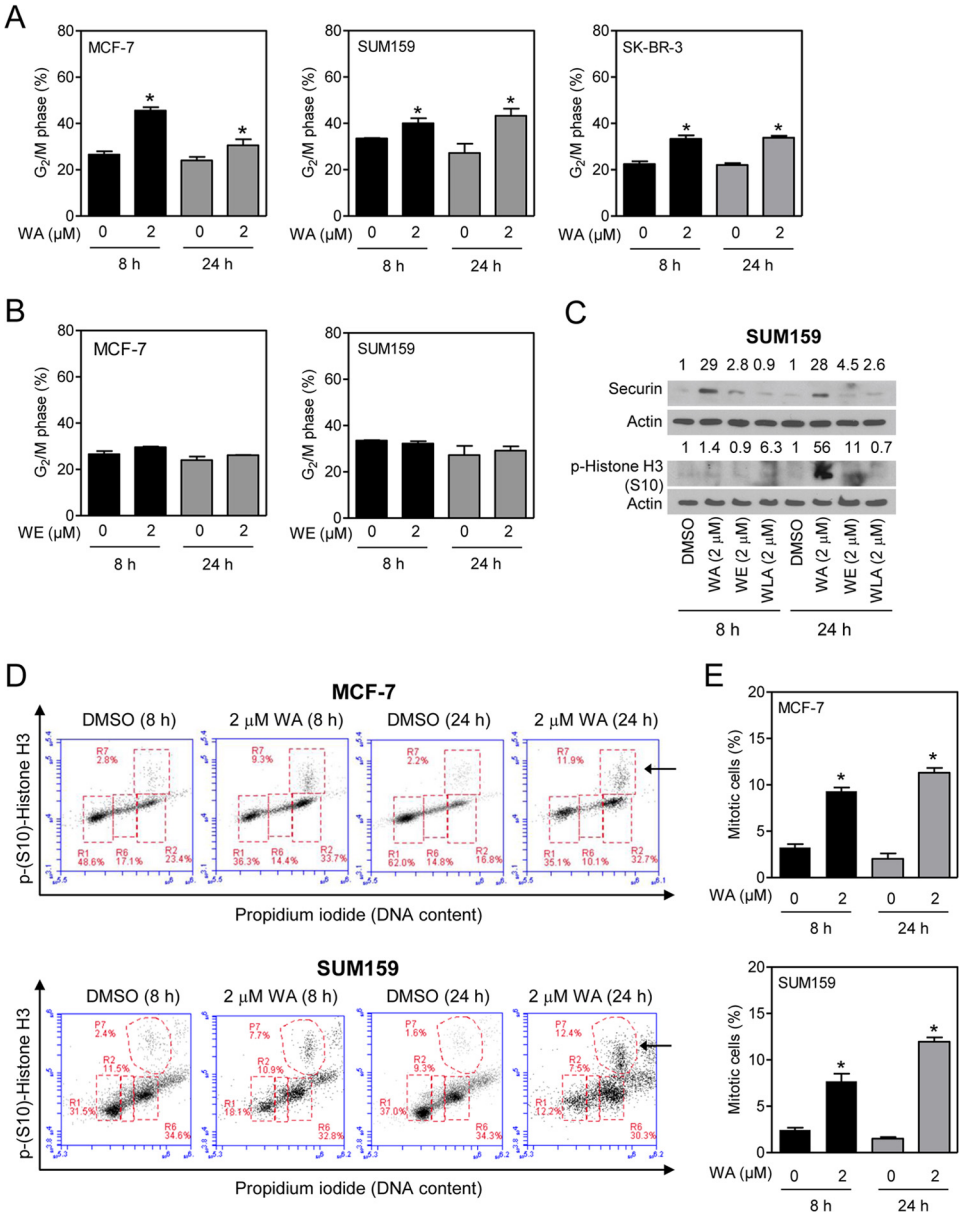

FIGURE 2. **WA treatment results in G_2 and mitotic arrest in human breast cancer cells.** *A*, effect of WA (8- or 24-h treatment) on G_2-M fractions in MCF-7, SUM159, and SK-BR-3 cells. *B*, effect of WE (8- or 24-h treatment) on G_2-M fractions in MCF-7 and SUM159 cells. *C*, Western blot analysis of securin and phospho-Ser[10] histone H3 using lysates from SUM159 cells treated for 8 or 24 h with DMSO (control) or WA, WE, or WLA (2 μM). The *numbers* on top of the bands represent changes in protein levels relative to the DMSO-treated control. *D*, representative flow histograms depicting mitotic fractions (identified by the *arrows*) from MCF-7 and SUM159 cells after a 8- or 24-h treatment with DMSO or 2 μM WA. *E*, quantitation of mitotic fractions in MCF-7 and SUM159 cells from the data shown in *D*. Results shown are means ± S.D. ($n = 2$–3). *, statistically significant ($p < 0.05$) compared with the DMSO control by Student's *t* test. Each experiment was repeated twice, and the results were comparable.

staining the cells with anti-α- and anti-β-tubulin antibodies (Fig. 5*A*). The DMSO-treated control MCF-7, SUM159, and SK-BR-3 cells exhibited a typical interphase microtubule network that extended throughout the cell; however, this network was severely disrupted after a 24-h WA treatment in each cell line (Fig. 5*A*).

Images for α- and β-tubulin in the mitotic spindle of MCF-7 cells were also acquired. Control cells showed a normal bipolar spindle with chromosomes aligned along the metaphase plate (Fig. 5*B*). In contrast, WA treatment led to a severe disruption of normal spindle morphology. Specifically, spindles did not contain clear poles, and the microtubules appeared disorganized and bundled (Fig. 5*B*). Chromosomes were also misaligned but still accumulated within the spindle. Additional confocal images of β-tubulin showed a similar trend, whereby WA treatment caused a complete disruption of normal spindle morphology and chromosome alignment (Fig. 5*B*). Collectively, these results indicated disruption of the microtubule network after treatment of MCF-7, SUM159, and SK-BR-3 cells with WA.

Effect of WA Treatment on Cell Cycle Distribution and Tubulin Expression in a Non-Tumorigenic Mammary Epithelial Cell Line—We used a spontaneously immortalized normal human mammary epithelial cell line (MCF-10A) that was established from fibrocystic breast disease rather than tumor to study the cancer cell selectivity of WA. The MCF-10A cells behaved differently from breast cancer cells with respect to WA-mediated

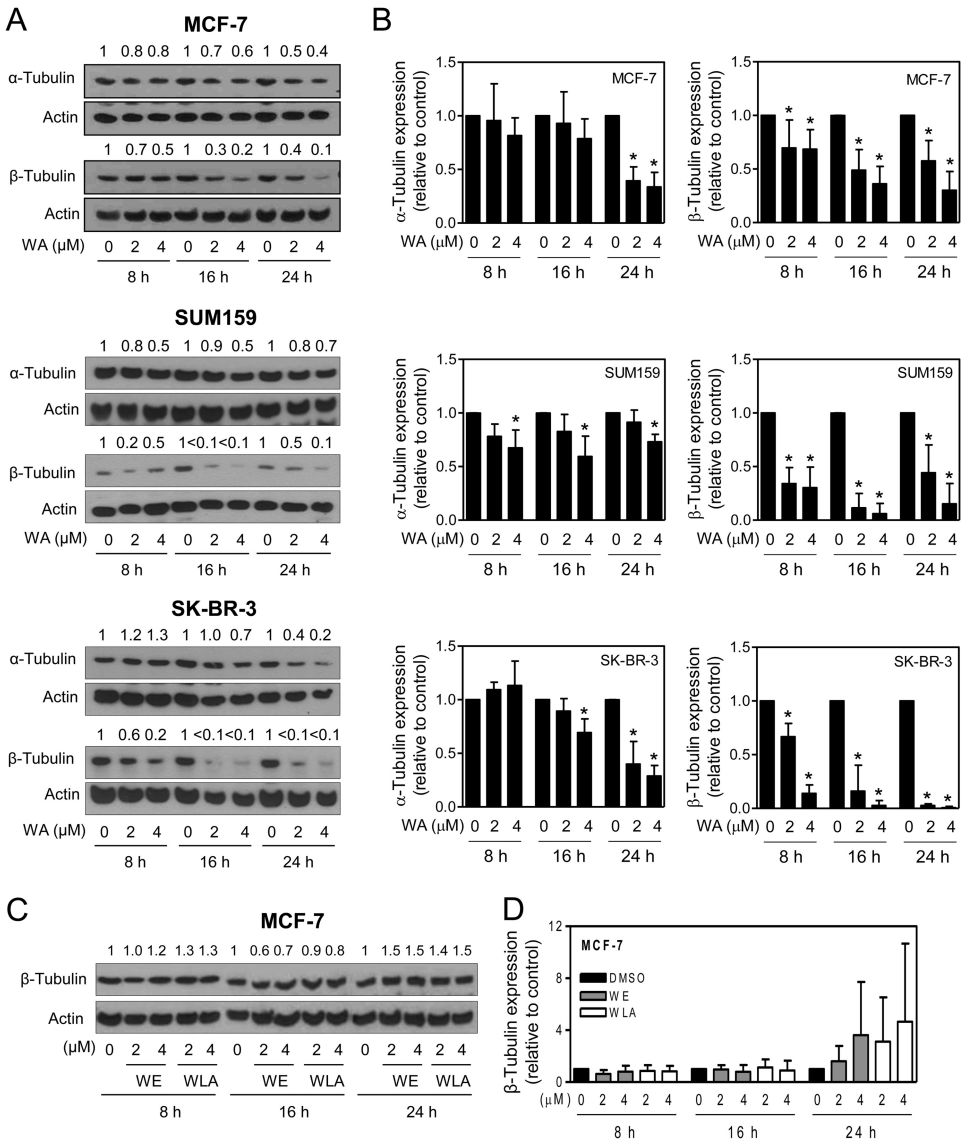

FIGURE 3. **WA treatment decreases the protein levels of α- and β-tubulin in human breast cancer cells.** *A*, representative immunoblots for α- and β-tubulin proteins using lysates from MCF-7, SUM159, and SK-BR-3 human breast cancer cells treated with DMSO or the indicated doses of WA for 8, 16, or 24 h. The change in tubulin protein levels relative to the corresponding DMSO control is shown on top of the bands. *B*, quantitation of tubulin protein expression. Results are shown as means ± S.D. ($n = 3–5$). *, significantly different ($p < 0.05$) compared with the corresponding DMSO control by one-way analysis of variance, followed by Dunnett's test. *C*, immunoblotting for β-tubulin using lysates from MCF-7 cells treated with DMSO or the indicated doses of WE or WLA for 8, 16, or 24 h. *D*, quantitation of the effects of WE and WLA treatments on β-tubulin protein expression in MCF-7 cells. Results shown are means ± S.D. ($n = 3–4$).

inhibition of cell cycle progression and tubulin expression. First, as shown in Fig. 6 (*A* and *B*), the WA-mediated G_2 and mitotic arrest was much less pronounced in MCF-10A cells than in breast cancer cells. Second, unlike breast cancer cells, the WA-mediated down-regulation of tubulin proteins at the pharmacological achievable dose of 2 μM was modest at best in MCF-10A cells (Fig. 6*C*). Finally, confocal microscopy revealed aggregation of β-tubulin around the nucleus in WA-treated MCF-10A cells (Fig. 6*D*), which was not obvious in breast cancer cells (Fig. 5*A*). Collectively, these results showed that a normal mammary epithelial cell line responded differently than breast cancer cells to WA-mediated cell cycle arrest.

Overexpression of Copper/Zinc Superoxide Dismutase Fails to Confer Protection against WA-mediated Decreases in Tubulin Proteins—Previous work from our laboratory has established a critical role for ROS in apoptotic cell death by WA in breast cancer cells (17). Therefore, it was of interest to determine whether the WA-mediated decline in tubulin protein was linked to ROS generation. A decrease in α- and β-tubulin protein levels after treatment with WA was observed not only in empty vector-transfected MCF-7 cells but also in MCF-7 cells overexpressing copper/zinc superoxide dismutase (data not shown). These results ruled out involvement of ROS in the WA-mediated decrease in tubulin protein levels.

Thiol Reactivity of Withanolides—The cysteine residues in tubulin are susceptible to electrophilic modifications (35). The chemical structures of the withanolides used in this study suggested three potential electrophilic sites for cysteine thiol additions. The irreversible modification of enzymes and receptors has been identified as a common mechanistic pathway for natural products as well as pharmaceuticals (36–39). The most reactive sites on withanolides appeared to be the A-ring enone

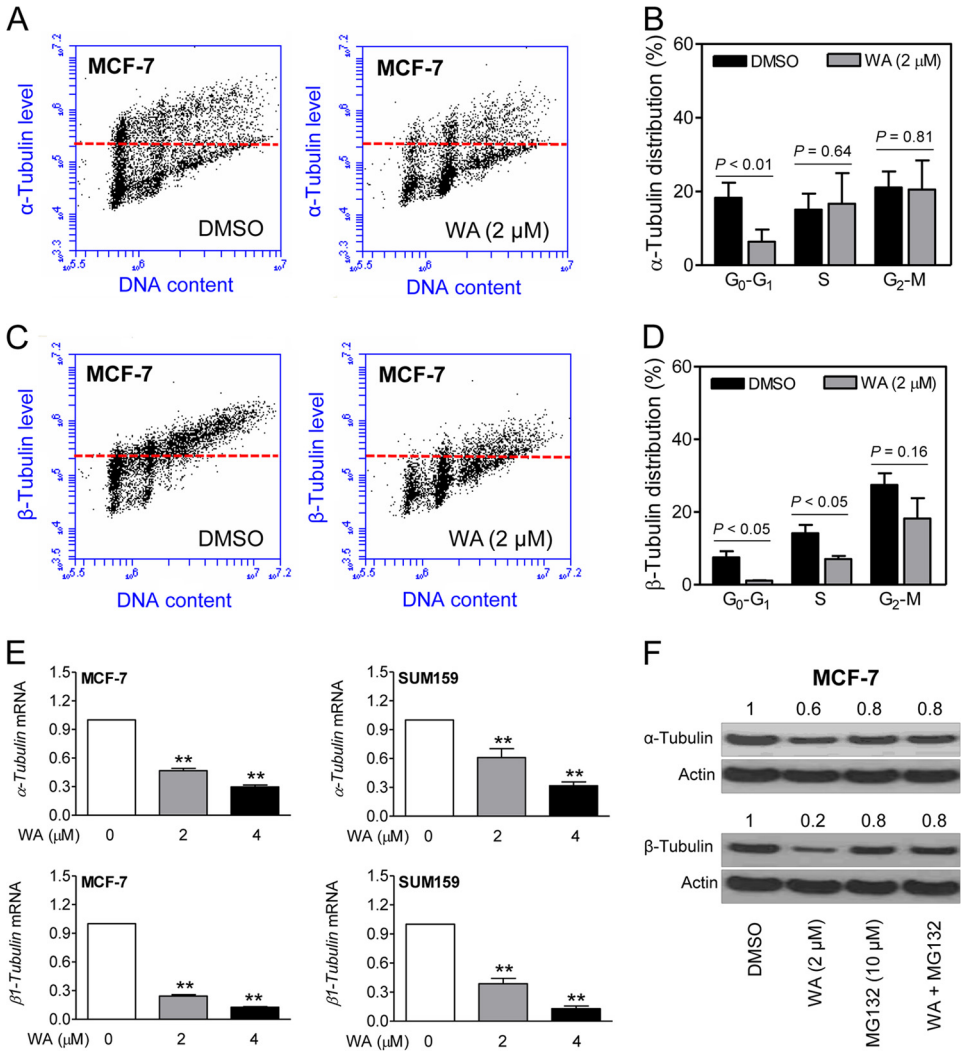

FIGURE 4. **Cell cycle phase-specific down-regulation of α- and β-tubulin by WA treatment.** *A*, representative flow histograms depicting cell cycle phase-specific expression of α-tubulin in MCF-7 cells treated with DMSO or 2 μM WA (24-h treatment). *B*, cell cycle phase-specific quantitation of α-tubulin is shown in the bar graph. *C*, representative flow histograms depicting cell cycle phase-specific expression of β-tubulin in MCF-7 cells treated with DMSO or 2 μM WA (24-h treatment). *D*, cell cycle phase-specific quantitation of β-tubulin is shown in the bar graph. Data represent means ± S.D. ($n = 3$). Statistical significance was determined by Student's *t* test. *E*, real-time quantitative RT-PCR for mRNA levels of α- and β_1-tubulin (*upper* and *lower panels*, respectively) in MCF-7 and SUM159 cells after a 24-h treatment with DMSO or the indicated concentrations of WA. Data represent means ± S.D. ($n = 3$). **, significantly different ($p < 0.01$) compared with the DMSO-treated control by one-way analysis of variance, followed by Dunnett's test. *F*, Western blotting for α- and β-tubulin using lysates from MCF-7 cells treated for 24 h with WA and/or MG132 (2-h pretreatment). The *numbers* on top of the bands represent the change in protein levels relative to the DMSO-treated control. Each experiment was repeated with comparable results.

and the B-ring oxirane, followed by the side chain enoate. However, the addition to the A-ring enone as well as the side chain enoate could be reversible and thermodynamically unfavorable (40–42). In WA, the epoxide attack would be slow due to the AB-ring conformation, forcing the nucleophile to add from the concave face of the decalin ring. In WE and WLA, the diaxial epoxide opening is expected to be slow due to steric hindrance from the axial methyl group. In WA, the A-ring enone features a hydroxyl group at the allylic position that would accelerate the cysteine addition. Based on prior studies (42), it is also likely that the *trans*-decalin enones in WE and WLA have less favorable equilibria for thiol capture than the *cis*-decalin enone in WA.

To test these hypotheses experimentally, we conducted NMR trapping experiments with cysteamine as the nucleophile (43). The results unambiguously confirmed that WA was the superior Michael acceptor (Fig. 7). Within 5 min after the addition of cysteamine to a solution of WA in DMSO-d_6, the enone signals at δ 7.08 and 6.12 ppm disappeared and did not reappear after 5 h or upon dilution in $CDCl_3$, indicating a fast and completely irreversible trapping reaction. In contrast, the corresponding enone signals in WLA decreased by only 25% after 5 min and reappeared in full intensity after 5 h, corresponding to a slow addition and a thermodynamically unfavorable process. For WE, the enone signal integrals remained unchanged after the cysteamine addition (Fig. 7), providing no evidence for thiol capture by this natural product. For both WLA and WE, diluting a sample in $CDCl_3$ did also not cause any change in the integration of the enone signals. Accordingly, the experimental measurements confirmed that WA represented a vastly superior electrophile compared with WLA or WE for irreversible thiol capture.

WA Binds Cys^{303} of Human β-Tubulin—Initially, we used purified human tubulin to study its possible interaction with

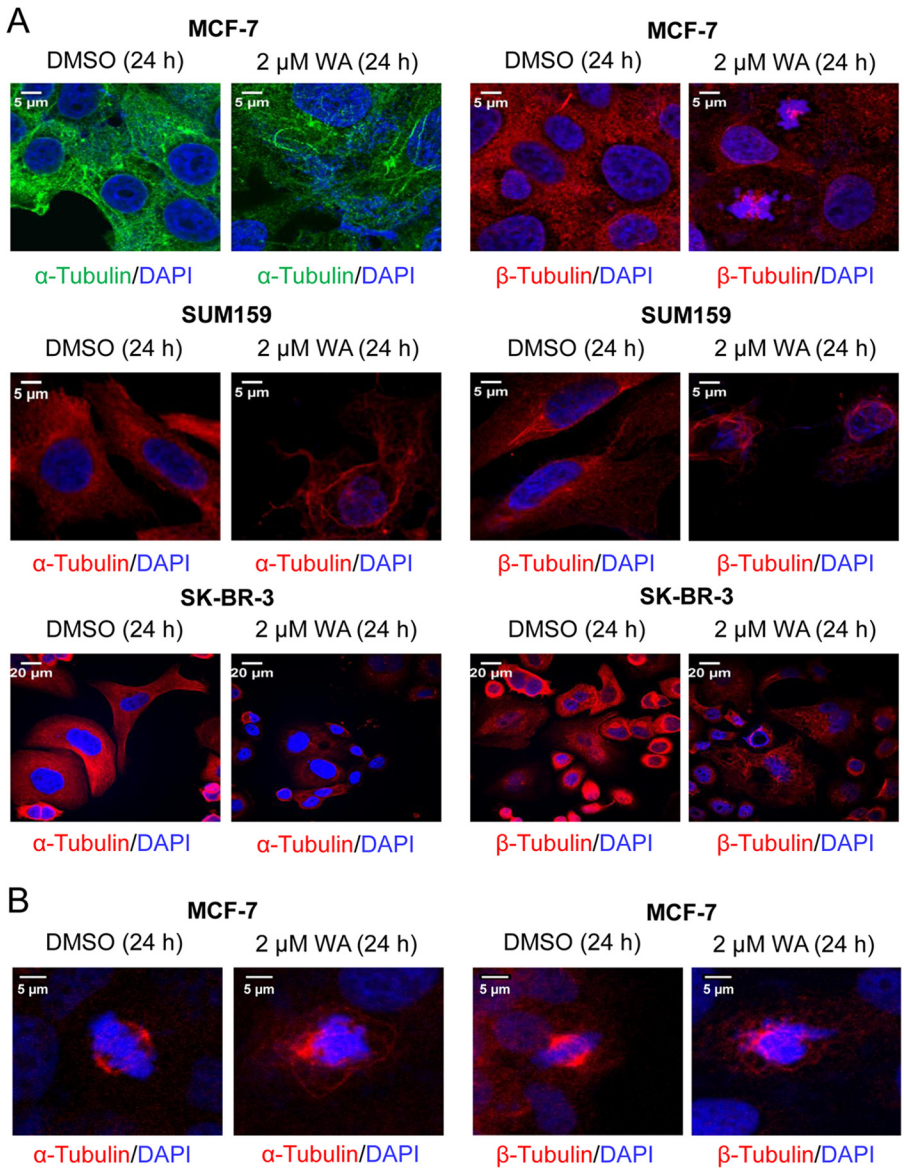

FIGURE 5. **WA disrupts microtubule organization and causes aberrant mitotic spindle morphology.** *A*, confocal images (×63 objective magnification (oil)) of α- and β-tubulin expression in interphase MCF-7, SUM159, and SK-BR-3 human breast cancer cells treated for 24 h with DMSO or 2 μM WA. *Scale bars* = 5 μm for MCF-7 and SUM159 cells and 20 μm for SK-BR-3 cells. *B*, confocal images of representative mitotic cells in MCF-7 cultures treated for 24 h with DMSO or 2 μM WA. Mitotic spindles were imaged using anti-α-tubulin or anti-β-tubulin antibody (*red*), and chromosomes were stained with DAPI (*blue*). *Scale bars* = 5 μm.

WA. Human β-tubulin contains eight cysteine residues. Using MALDI-TOF, we were able to reproducibly detect four ions that matched the predicted monoisotopic *m/z* of four cysteine-containing peptides. Data-dependent LC-MS/MS analysis confirmed the sequences of three cysteine-containing peptides to be EIVHLQAGQC^{12}GNQIGAK, NMMAAC^{303}DPR, and TAVC^{354}DIPPR. MALDI-TOF analysis revealed formation of two ions at *m/z* 971.51 and 1441.77 that corresponded to the *m/z* of TAVC^{354}DIPPR with and without the addition of WA (470.6 Da). To obtain site-specific evidence of WA adduct formation, we performed a series of data-dependent LC-MS/MS analyses. For purified tubulin treated with WA *in vitro*, the peptides at *m/z* 747.838^{2+} and 512.704^{2+} were detected in the high-resolution full-scan spectra, and their masses corresponded to WA adduction to Cys^{303} of NMMAAC^{303}DPR and also the unmodified form of the peptide. In the control sample, only the unmodified form was detected (data not shown). MS/MS analysis revealed the formation of a covalent bond with Cys^{303}, and the mass of the resulting tryptic peptide (NMM(ox)-AAC(WA)DPR) had increased by the molecular weight of WA. Evidence of WA adduct formation at the six remaining cysteine residues was not observed, indicating that these sites are either not modified or not observed by our experimental approach. Similarly, covalent addition of WE and WLA was not observed with any cysteine when purified tubulin was treated with these agents *in vitro* (data not shown).

In a separate experiment, we studied the WA binding to Cys^{303} using MCF-7 cells. For these studies, MCF-7 cells were treated with 2 μM WA or DMSO (control) for 24 h. The cells were then lysed, and β-tubulin was enriched by immunoprecipitation. LC-MS/MS was used to measure the relative abundance of seven tryptic peptide sequences that comprise the

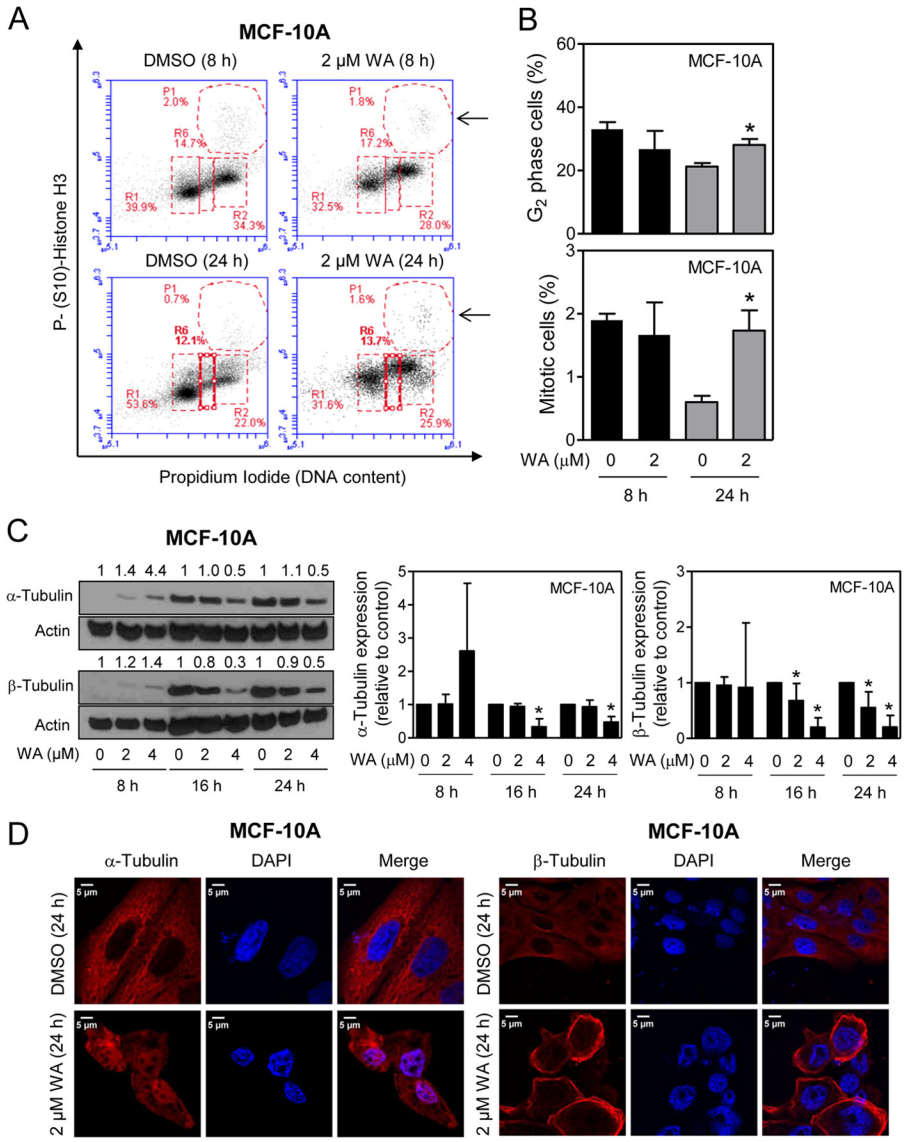

FIGURE 6. **MCF-10A cells are relatively less sensitive to WA-mediated mitotic arrest compared with breast cancer cells.** *A*, representative flow histograms depicting cell cycle distribution in MCF-10A cells after a 8- or 24-h treatment with DMSO or 2 μM WA. Mitotic fraction are identified by *arrows*. *B*, quantitation of G_2 and mitotic cells from data shown in *A*. Results shown are means ± S.D. ($n = 3$). *, statistically significant ($p < 0.05$) compared with the control by Student's *t* test. *C*, quantitation of the effect of WA treatment (8, 16, or 24 h) on the protein levels of α- and β-tubulin determined by Western blotting. Results shown are means ± S.D. ($n = 3$–5). *, significantly different ($p < 0.05$) compared with the vehicle-treated control by one-way analysis of variance with Dunnett's adjustment. *D*, confocal images (×63 objective magnification (oil)) depicting the effect of WA treatment (24 h) on α- and β-tubulin protein expression in interphase MCF-10A cells. *Scale bars* = 5 μm. Results were comparable in replicate experiments.

eight cysteine residues in β-tubulin. The tandem mass spectra for the modified and unmodified NMM#AACDPR peptides containing Cys^{303} are shown in Fig. 8 (*A* and *B*, respectively). The relative abundance of this peptide in samples derived from MCF-7 cells (Fig. 8*C*) was determined by integrating the b_7^+ ion intensity. These results demonstrated that the Cys^{303} modification of β-tubulin was detected in the WA-treated MCF-7 cells but not in the DMSO-treated cells.

Model of the Cys^{303}-WA Adduct of Human β-Tubulin—The WA-binding pocket is located on the surface of human β-tubulin (Fig. 9*A*, *left*). It has a hydrophobic floor, a hydrophobic wall, and a charge-balanced hydrophilic entrance (Fig. 9*A*, *right*). A network of electrostatic and hydrogen bonding interactions formed between alternately charged amino acid side chains makes the WA-binding pocket well defined and relatively stable. Glu^{205}, Ala^{206}, Asp^{209}, Ile^{210}, Arg^{213}, Lys^{297}, Ala^{302}, and Arg^{380} of human β-tubulin are involved in hydrophobic interactions with the Cys^{303}-WA adduct. The guanidinium group of Arg^{213} is also involved in electrostatic interactions with the WA moiety, forming the only hydrogen bond with the Cys^{303}-WA adduct (Fig. 9*A*, *right*). Two additional hydrogen bonding interactions were observed between WA and the side chains of Arg^{380} and Thr^{214} in human β-tubulin in the protein-substrate model (data not shown). These electrostatic interactions may be required to sequester the WA molecule into the WA-binding pocket for Cys^{303}-WA adduct formation.

DISCUSSION

Microtubules are hollow cylindrical structures that radiate from the microtubule-organizing centrosomes of interphase

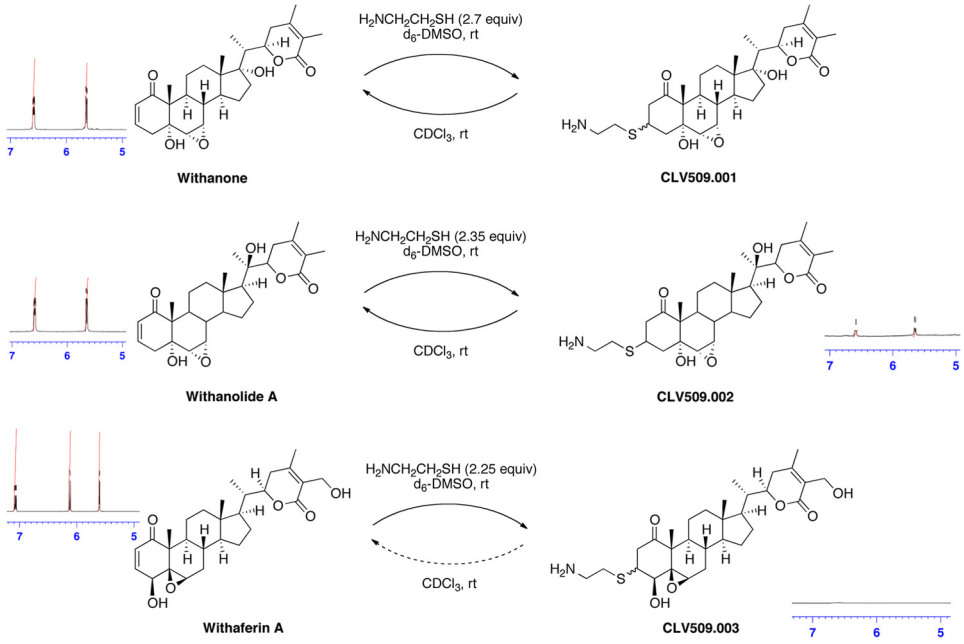

FIGURE 7. **Thiol reactivity of withanolides determined by NMR.** Shown are the results of NMR trapping experiments with cysteamine as the nucleophile and WE, WLA, and WA as electrophiles. For WE, no difference was observed at the enone peaks at 6.58 and 5.64 ppm. For WLA, the enone peaks at 6.58 and 5.64 ppm decreased by 25% after 5 min of incubation, but these peaks were present in full intensity after 5 h. For WA, the enone peaks at 7.08 and 6.12 ppm disappeared 5 min after thiol addition and did not reappear. Thus, only WA resulted in an irreversible addition of the thiol to the enone moiety.

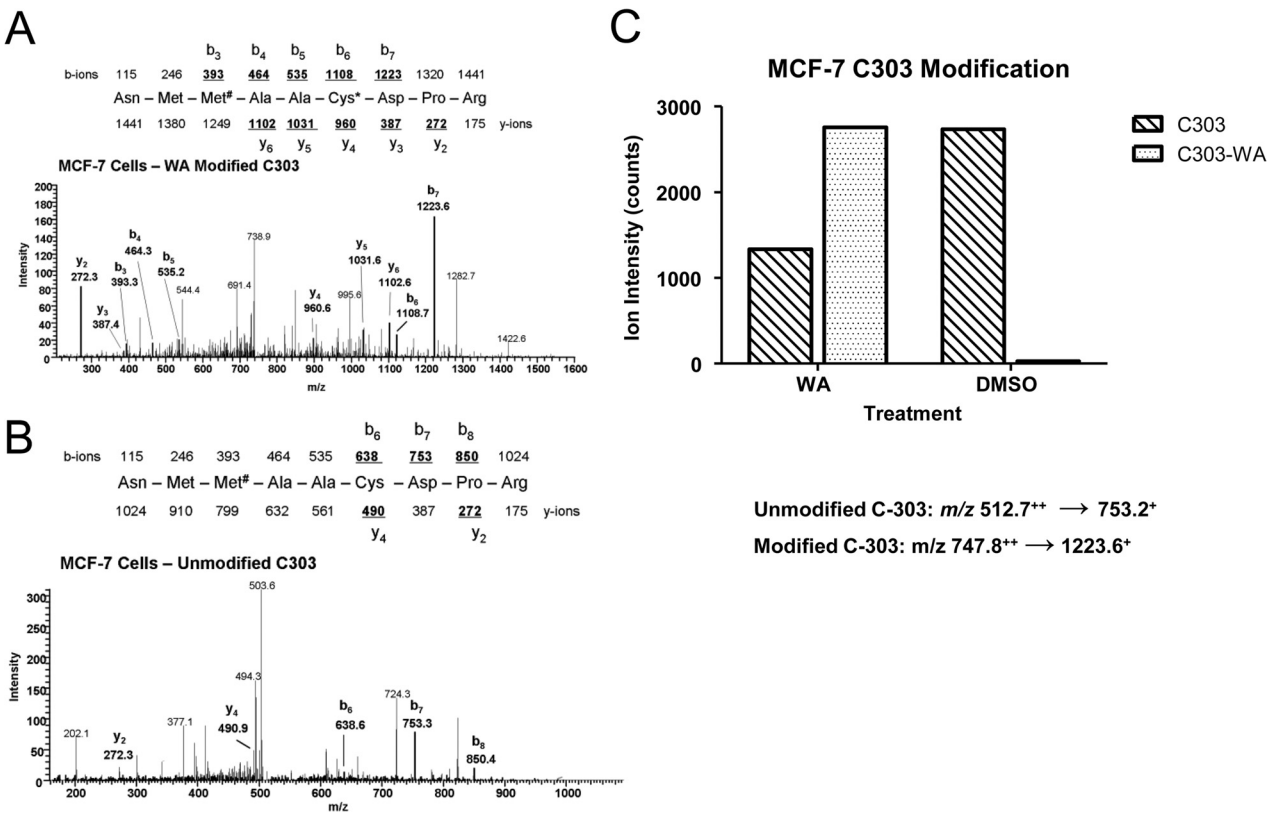

FIGURE 8. **Sequence-specific quantitation of the modified and unmodified tryptic peptides (NMMAACDPR) in MCF-7 cells treated with WA and DMSO.** *A*, tandem mass spectrum of peptide NMM#AAC(WA)DPR with sequence-specific product ions (b_6 and y_4), confirming the presence of the Cys^{303}-WA adduct. *B*, tandem mass spectrum of the unmodified NMMAACDPR peptide in samples derived from MCF-7 cells incubated with DMSO. *C*, quantitation of the b_7^+ product ion in MCF-7 cells treated with WA and DMSO.

cells (44). The microtubule network is composed of α- and β-tubulin heterodimers that are critical for cell cycle progression (mitosis), cellular movement, and intracellular trafficking (45). Microtubules have remained an attractive target for cancer chemotherapy as exemplified by the clinical success of antimitotic agents, including vinca alkaloids and taxanes (34, 44).

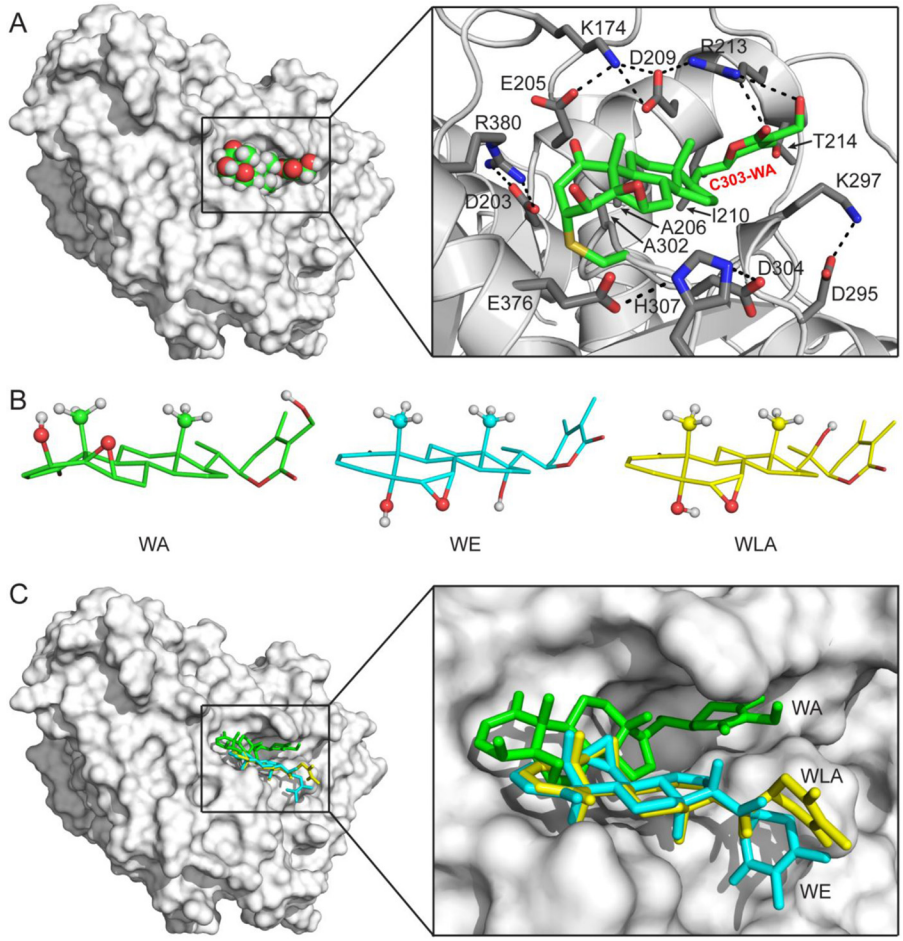

FIGURE 9. **Docking of the Cys^{303}-WA adduct in human β-tubulin.** *A*, model of the Cys^{303}-WA adduct of human β-tubulin. *Left*, overall view of the model. The human β-tubulin model is shown as a molecule surface, and the Cys^{303}-WA adduct is shown as a sphere model with an atomic color scheme (carbon in *green*, oxygen in *red*, and hydrogen in *white*). *Right*, details of the WA-binding pocket. The human β-tubulin model is shown as a ribbon diagram (helices as *spirals*, strands as *arrows*, and loops as *tubes*) with WA-interacting side chains as sticks (nitrogen in *blue*, carbon in *gray*, and oxygen in *red*), and the Cys^{303}-WA adduct is shown as a stick model (nitrogen in *blue*, carbon in *green*, oxygen in *red*, and sulfur in *yellow*). Hydrogen atoms are not shown for clarity. *B*, comparison of the WA, WE, and WLA structures (PubChem Database SID 11034, 103600366, and 103600367, respectively). The three structures are aligned on the basis of their fused rings. Free rotations around side chain single bonds are allowed. For clarity, hydrogen atoms are shown for the hydroxyl and axial methyl groups only. *C*, WE and WLA are not compatible for Cys^{303} adduct formation with human β-tubulin. *Left*, overall view showing the docked position of WA (in *green*), WE (in *cyan*), or WLA (in *yellow*). *Right*, enlarged view shows that WE and WLA cannot be docked into the WA-binding pocket.

The results presented herein indicate, for the first time, that tubulin is a novel target of growth arrest by WA. Expression of both α- and β-tubulin proteins is markedly decreased upon treatment of human breast cancer cells with a pharmacologically relevant concentration of WA regardless of the ER or human EGF receptor-2 status.

It is important to point out that a non-tumorigenic normal mammary epithelial cell line is relatively less sensitive to these effects of WA compared with breast cancer cells. These observations complement our prior published findings demonstrating marked resistance of normal mammary epithelial cells to apoptosis induction by WA in comparison with breast cancer cells (12, 17).

The naturally occurring C_6,C_7-epoxy derivatives of WA (WE and WLA) neither cause growth arrest nor suppress the levels of α- or β-tubulin, suggesting that the location of the epoxide functional group is critical for the tubulin-targeting effect of withanolides. Down-regulation of tubulin proteins after WA treatment involves transcriptional repression as well as proteasomal degradation. Similar to other tubulin- and microtubule-targeting agents (34, 44), WA treatment results in G_2-M phase cell cycle arrest and aberrant microtubule spindle formation. However, the spindle morphology after WA treatment differs from that in cells treated with taxanes, which cause multipolar spindles (46), or Eg5 inhibitors, which cause monopolar spindles (47). Instead, the WA-treated breast cancer cells have severely disrupted spindle morphology without a well defined spindle pole. Interestingly, the β-tubulin protein is relatively more sensitive to down-regulation upon WA treatment compared with α-tubulin, but the mechanism underlying this differential response remains unclear.

Cysteine-rich tubulins are susceptible to modification by structurally diverse small molecules (48, 49). For example, the G_2-M phase cell cycle arrest in human colon cancer cells upon treatment with a garlic-derived sulfur compound (diallyl trisulfide) was shown to be associated with oxidation of Cys^{12} and Cys^{354} of β-tubulin (*S*-allylmercaptocysteine adduct) in a cell-free system (48). Formation of these adducts after treatment of cells with diallyl trisulfide was not shown (48). The incubation of purified porcine α- and β-tubulin with allyl isothiocyanate, a

component of mustard, resulted in covalent adduction at Cys^{127}, Cys^{347}, and Cys^{376} of α-tubulin and Cys^{12}, Cys^{239}, Cys^{303}, and Cys^{354} of β-tubulin (49). However, these covalent interactions were thought to be reversible because no such adducts were detectable after treatment of the UM-UC-3 human bladder cancer cell line with allyl isothiocyanate (49). In this study, we have demonstrated that WA covalently binds Cys^{303} of β-tubulin in a cell-free system as well as in MCF-7 cells. Presently, it is still unclear if the cysteine residues in the α-tubulin protein are susceptible to covalent modification by WA. Nevertheless, the molecular docking simulations confirmed the stability of the Cys^{303}-WA adduct in the pocket.

WE and WLA are unable to attack Cys^{303} or any other cysteine residue in β-tubulin even in a cell-free system. Structure alignments of WA, WE, and WLA on the basis of the fused ring system show a significant difference between WA and its analogs. In WA, the hydroxyl, epoxy, and axial methyl groups on the fused rings are clustered on one side of the system, whereas they are distributed on both sides in WE and WLA (Fig. 9*B*). As mentioned above, the WA-binding pocket has a hydrophobic floor. The WA molecule fits in the pocket with its "flat bottom" against the floor (Fig. 9*A*), which positions the A-ring enone β-carbon in close proximity to the Cys^{303}-SH group. In contrast, WE and WLA molecules do not have such a flat bottom, and the steric conflict due to their hydroxyl, epoxy, and axial methyl groups on the fused rings prohibits their docking into the WA-binding pocket, not to mention positioning their enone β-carbon near the Cys^{303} side chain (Fig. 9*C*).

Research over the past 5–7 years has established that WA inhibits multiple cellular pathways (*e.g.* ER-α, NF-κB, and STAT3) and processes (angiogenesis and cancer cell migration and invasion) relevant to cancer development (18–22). Inhibition of complex III of mitochondrial respiration, triggering ROS production and leading to activation of Bak, is an important mechanism by which this agent causes apoptotic cell death (17). On one hand, lack of target specificity is a perceived weakness of naturally occurring anticancer agents, and WA is no exception to this potential criticism. On the other hand, ability to target multiple pathways and processes is a desirable attribute because the pathogenesis of cancer is complex, often characterized by deregulation of multiple checkpoints and activation of several oncogenic pathways. Agents selective against a single pathway/molecule may have limited clinical utility as exemplified by the ER antagonists for prevention of breast cancer (50). We are also tempted to speculate that many of the effects of WA (*e.g.* inhibition of complex III, NF-κB, and STAT3) may be due to its ability to target specific cysteine residue(s) on these proteins. Experimental validation of this hypothesis awaits further investigation. In conclusion, in this study, we have not only identified β-tubulin as a novel target of growth arrest by WA but also have shed light on the elements in the withanolide structure (*e.g.* location of the epoxide functional group and relative reactivity of the enone Michael acceptor *versus* other withanolides) responsible for its electrophilic and tubulin-targeting effects.

REFERENCES

1. Aggarwal, B. B., Prasad, S., Reuter, S., Kannappan, R., Yadev, V. R., Park, B., Kim, J. H., Gupta, S. C., Phromnoi, K., Sundaram, C., Prasad, S., Chaturvedi, M. M., and Sung, B. (2011) Identification of novel anti-inflammatory agents from Ayurvedic medicine for prevention of chronic diseases: "reverse pharmacology" and "bedside to bench" approach. *Curr. Drug Targets* **12,** 1595–1653
2. Mishra, L. C., Singh, B. B., and Dagenais, S. (2000) Scientific basis for the therapeutic use of *Withania somnifera* (ashwagandha): a review. *Altern. Med. Rev.* **5,** 334–346
3. Widodo, N., Kaur, K., Shrestha, B. G., Takagi, Y., Ishii, T., Wadhwa, R., and Kaul, S. C. (2007) Selective killing of cancer cells by leaf extract of ashwagandha: identification of a tumor-inhibitory factor and the first molecular insights to its effect. *Clin. Cancer Res.* **13,** 2298–2306
4. Padmavathi, B., Rath, P. C., Rao, A. R., and Singh, R. P. (2005) Roots of *Withania somnifera* inhibit forestomach and skin carcinogenesis in mice. *Evid. Based Complement Alternat. Med.* **2,** 99–105
5. Ichikawa, H., Takada, Y., Shishodia, S., Jayaprakasam, B., Nair, M. G., and Aggarwal, B. B. (2006) Withanolides potentiate apoptosis, inhibit invasion, and abolish osteoclastogenesis through suppression of nuclear factor-κB (NF-κB) activation and NF-κB-regulated gene expression. *Mol. Cancer Ther.* **5,** 1434–1445
6. Matsuda, H., Murakami, T., Kishi, A., and Yoshikawa, M. (2001) Structures of withanosides I, II, III, IV, V, VI, and VII, new withanolide glycosides, from the roots of Indian *Withania somnifera* DUNAL, and inhibitory activity for tachyphylaxis to clonidine in isolated guinea-pig ileum. *Bioorg. Med. Chem.* **9,** 1499–1507
7. Vyas, A. R., and Singh, S. V. (2013) Molecular targets and mechanisms of cancer prevention and treatment by withaferin A, a naturally occurring steroidal lactone. *AAPS J.* 10.1208/s12248-013-9531-1
8. Shohat, B., and Joshua, H. (1971) Effect of withaferin A on Ehrlich ascites tumor cells. II. Target tumor cell destruction *in vivo* by immune activation. *Int. J. Cancer* **8,** 487–496
9. Devi, P. U., Akagi, K., Ostapenko, V., Tanaka, Y., and Sugahara, T. (1996) Withaferin A: a new radiosensitizer from the Indian medicinal plant *Withania somnifera*. *Int. J. Radiat. Biol.* **69,** 193–197
10. Srinivasan, S., Ranga, R. S., Burikhanov, R., Han, S. S., and Chendil, D. (2007) Par-4-dependent apoptosis by the dietary compound withaferin A in prostate cancer cells. *Cancer Res.* **67,** 246–253
11. Yang, H., Shi, G., and Dou, Q. P. (2007) The tumor proteasome is a primary target for the natural anticancer compound withaferin A isolated from "Indian winter cherry". *Mol. Pharmacol.* **71,** 426–437
12. Stan, S. D., Hahm, E. R., Warin, R., and Singh, S. V. (2008) Withaferin A causes FOXO3a- and Bim-dependent apoptosis and inhibits growth of human breast cancer cells *in vivo*. *Cancer Res.* **68,** 7661–7669
13. Manoharan, S., Panjamurthy, K., Menon, V. P., Balakrishnan, S., and Alias, L. M. (2009) Protective effect of withaferin-A on tumour formation in 7,12-dimethylbenz[*a*]anthracene induced oral carcinogenesis in hamsters. *Indian J. Exp. Biol.* **47,** 16–23
14. Hahm, E. R., Lee, J., Kim, S. H., Sehrawat, A., Arlotti, J. A., Shiva, S. S., Bhargava, R., and Singh, S. V. (2013) Metabolic alterations in mammary cancer prevention by withaferin A in a clinically relevant mouse model. *J. Natl. Cancer Inst.* **105,** 1111–1122
15. Thaiparambil, J. T., Bender, L., Ganesh, T., Kline, E., Patel, P., Liu, Y., Tighiouart, M., Vertino, P. M., Harvey, R. D., Garcia, A., and Marcus, A. I. (2011) Withaferin A inhibits breast cancer invasion and metastasis at subcytotoxic doses by inducing vimentin disassembly and serine 56 phosphorylation. *Int. J. Cancer* **129,** 2744–2755
16. Stan, S. D., Zeng, Y., and Singh, S. V. (2008) Ayurvedic medicine constituent withaferin A causes G_2 and M phase cell cycle arrest in human breast cancer cells. *Nutr. Cancer* **60,** 51–60
17. Hahm, E. R., Moura, M. B., Kelley, E. E., Van Houten, B., Shiva, S., and Singh, S. V. (2011) Withaferin A-induced apoptosis in human breast cancer cells is mediated by reactive oxygen species. *PLoS ONE* **6,** e23354
18. Kaileh, M., Vanden Berghe, W., Heyerick, A., Horion, J., Piette, J., Libert, C., De Keukeleire, D., Essawi, T., and Haegeman, G. (2007) Withaferin a strongly elicits IκB kinase β hyperphosphorylation concomitant with po-

tent inhibition of its kinase activity. *J. Biol. Chem.* **282,** 4253–4264
19. Lee, J., Hahm, E. R., and Singh, S. V. (2010) Withaferin A inhibits activation of signal transducer and activator of transcription 3 in human breast cancer cells. *Carcinogenesis* **31,** 1991–1998
20. Hahm, E. R., Lee, J., Huang, Y., and Singh, S. V. (2011) Withaferin A suppresses estrogen receptor-α expression in human breast cancer cells. *Mol. Carcinog.* **50,** 614–624
21. Mohan, R., Hammers, H. J., Bargagna-Mohan, P., Zhan, X. H., Herbstritt, C. J., Ruiz, A., Zhang, L., Hanson, A. D., Conner, B. P., Rougas, J., and Pribluda, V. S. (2004) Withaferin A is a potent inhibitor of angiogenesis. *Angiogenesis* **7,** 115–122
22. Lee, J., Sehrawat, A., and Singh, S. V. (2012) Withaferin A causes activation of Notch2 and Notch4 in human breast cancer cells. *Breast Cancer Res. Treat.* **136,** 45–56
23. Xiao, D., Vogel, V., and Singh, S. V. (2006) Benzyl isothiocyanate-induced apoptosis in human breast cancer cells is initiated by reactive oxygen species and regulated by Bax and Bak. *Mol. Cancer Ther.* **5,** 2931–2945
24. Xiao, D., Choi, S., Johnson, D. E., Vogel, V. G., Johnson, C. S., Trump, D. L., Lee, Y. J., and Singh, S. V. (2004) Diallyl trisulfide-induced apoptosis in human prostate cancer cells involves c-Jun N-terminal kinase and extracellular signal regulated kinase-mediated phosphorylation of Bcl-2. *Oncogene* **23,** 5594–5606
25. Xiao, D., Srivastava, S. K., Lew, K. L., Zeng, Y., Hershberger, P., Johnson, C. S., Trump, D. L., and Singh, S. V. (2003) Allyl isothiocyanate, a constituent of cruciferous vegetables, inhibits proliferation of human prostate cancer cells by causing G_2/M arrest and inducing apoptosis. *Carcinogenesis* **24,** 891–897
26. Livak, K. J., and Schmittgen, T. D. (2001) Analysis of relative gene expression data using real-time quantitative PCR and the $2^{-\Delta\Delta CT}$ method. *Methods* **25,** 402–408
27. Shevchenko, A., Tomas, H., Havlis, J., Olsen, J. V., and Mann, M. (2006) In-gel digestion for mass spectrometric characterization of proteins and proteomes. *Nat. Protoc.* **1,** 2856–2860
28. Prota, A. E., Magiera, M. M., Kuijpers, M., Bargsten, K., Frey, D., Wieser, M., Jaussi, R., Hoogenraad, C. C., Kammerer, R. A., Janke, C., and Steinmetz, M. O. (2013) Structural basis of tubulin tyrosination by tubulin tyrosine ligase. *J. Cell Biol.* **200,** 259–270
29. Kelley, L. A., and Sternberg, M. J. E. (2009) Protein structure prediction on the Web: a case study using the Phyre server. *Nat. Protoc.* **4,** 363–371
30. Morris, G. M., Huey, R., Lindstrom, W., Sanner, M. F., Belew, R. K., Goodsell, D. S., and Olson, A. J. (2009) Autodock4 and AutoDockTools4: automated docking with selective receptor flexibility. *J. Comput. Chem.* **30,** 2785–2791
31. Bayraktar, S., and Glück, S. (2013) Molecularly targeted therapies for metastatic triple-negative breast cancer. *Breast Cancer Res. Treat.* **138,** 21–35
32. Hendzel, M. J., Wei, Y., Mancini, M. A., Van Hooser, A., Ranalli, T., Brinkley, B. R., Bazett-Jones, D. P., and Allis, C. D. (1997) Mitosis-specific phosphorylation of histone H3 initiates primarily within pericentromeric heterochromatin during G_2 and spreads in an ordered fashion coincident with mitotic chromosome condensation. *Chromosoma* **106,** 348–360
33. Peters, J. M. (2002) The anaphase-promoting complex: proteolysis in mitosis and beyond. *Mol. Cell* **9,** 931–943
34. Jordan, M. A., and Wilson, L. (2004) Microtubules as a target for anticancer drugs. *Nat. Rev. Cancer* **4,** 253–265
35. Luduena, R. F., and Roach, M. C. (1991) Tubulin sulfhydryl groups as probes and targets for antimitotic and antimicrotubule agents. *Pharmacol. Ther.* **49,** 133–152
36. Amslinger S. (2010) The tunable functionality of α,β-unsaturated carbonyl compounds enables their differential application in biological systems. *Chem. Med. Chem.* **5,** 351–356
37. Singh, J., Petter, R. C., Baillie, T. A., and Whitty, A. (2011) The resurgence of covalent drugs. *Nat. Rev. Drug Discov.* **10,** 307–317
38. Zheng, S., Santosh Laxmi, Y. R., David, E., Dinkova-Kostova, A. T., Shiavoni, K. H., Ren, Y., Zheng, Y., Trevino, I., Bumeister, R., Ojima, I., Wigley, W. C., Bliska, J. B., Mierke, D. F., and Honda, T. (2012) Synthesis, chemical reactivity as Michael acceptors, and biological potency of monocyclic cyanoenones, novel and highly potent anti-inflammatory and cytoprotective agents. *J. Med. Chem.* **55,** 4837–4846
39. Serafimova, I. M., Pufall, M. A., Krishnan, S., Duda, K., Cohen, M. S., Maglathlin, R. L., McFarland, J. M., Miller, R. M., Frödin, M., and Taunton, J. (2012) Reversible targeting of noncatalytic cysteines with chemically tuned electrophiles. *Nat. Chem. Biol.* **8,** 471–476
40. van Axel Castelli, V., Bernardi, F., Dalla Cort, A., Mandolini, L., Rossi, I., and Schiaffino, L. (1999) Rates and equilibria of the Michael-type addition of benzenethiol to 2-cyclopenten-1-ones. *J. Org. Chem.* **64,** 8122–8126
41. Krenske, E. H., Petter, R. C., Zhu, Z., and Houk, K. N. (2011) Transition states and energetics of nucleophilic additions of thiols to substituted α,β-unsaturated ketones: substituent effects involve enone stabilization, product branching, and solvation. *J. Org. Chem.* **76,** 5074–5081
42. Rosenker, C. J., Krenske, E. H., Houk, K. N., and Wipf, P. (2013) Influence of base and structure in the reversible covalent conjugate addition of thiol to polycyclic enone scaffolds. *Org. Lett.* **15,** 1076–1079
43. Avonto, C., Taglialatela-Scafati, O., Pollastro, F., Minassi, A., Di Marzo, V., De Petrocellis, L., and Appendino, G. (2011) An NMR spectroscopic method to identify and classify thiol-trapping agents: revival of Michael acceptors for drug discovery? *Angew. Chem. Int. Ed.* **50,** 467–471
44. Kavallaris, M. (2010) Microtubules and resistance to tubulin-binding agents. *Nat. Rev. Cancer* **10,** 194–204
45. Verhey, K. J., and Gaertig, J. (2007) The tubulin code. *Cell Cycle* **6,** 2152–2160
46. Chen, J. G., and Horwitz, S. B. (2002) Differential mitotic response to microtubule-stabilizing and destabilizing drugs. *Cancer Res.* **62,** 1935–1938
47. Marcus, A. I., Peters, U., Thomas, S. L., Garrett, S., Zelnak, A., Kapoor, T. M., and Giannakakou, P. (2005) Mitotic kinesin inhibitors induce mitotic arrest and cell death in Taxol-resistant and -sensitive cancer cells. *J. Biol. Chem.* **280,** 11569–11577
48. Hosono, T., Fukao, T., Ogihara, J., Ito, Y., Shiba, H., Seki, T., and Ariga, T. (2005) Diallyl trisulfide suppresses the proliferation and induces apoptosis of human colon cancer cells through oxidative modification of β-tubulin. *J. Biol. Chem.* **280,** 41487–41493
49. Geng, F., Tang, L., Li, Y., Yang, L., Choi, K. S., Kazim, A. L., and Zhang, Y. (2011) Allyl isothiocyanate arrests cancer cells in mitosis, and mitotic arrest in turn leads to apoptosis via Bcl-2 protein phosphorylation. *J. Biol. Chem.* **286,** 32259–32267
50. Fisher, B., Costantino, J. P., Wickerham, D. L., Redmond, C. K., Kavanah, M., Cronin, W. M., Vogel, V., Robidoux, A., Dimitrov, N., Atkins, J., Daly, M., Wieand, S., Tan-Chiu, E., Ford, L., and Wolmark, N. (1998) Tamoxifen for prevention of breast cancer: report of the National Surgical Adjuvant Breast and Bowel Project P-1 Study. *J. Natl. Cancer Inst.* **90,** 1371–1388